Experimental Determination and Modeling of Material Damping

Prof. Dr.-Ing. habil. **L. Gaul**, Dr.-Ing. **A. Schmidt**,
Institut für Angewandte und Experimentelle Mechanik, Stuttgart

Abstract

A structure's damping behavior is mainly influenced by the dissipative characteristics of its joints and the damping properties of its component materials. Part 2 of the VDI 3830 guideline damping of materials and members is dedicated to the modeling of linear and non-linear material damping while part 5 deals with different experimental techniques aiming at the extraction of appropriate material parameters. This paper gives an overview concerning the phenomena associated with linear viscoelastic material behavior and the respective modeling using classical derivatives and its generalization by the concept of fractional derivatives.

As an example, experimental investigations conducted on an engineering plastic material yield its temperature und frequency dependent material properties. Based on the principle of thermorheologic simple material behavior, a so-called master curve is identified which maps the elastic and the dissipative properties of the material over an extensive frequency range. Finally, the material behavior is efficiently modeled with few material parameters through the use of fractional derivatives. The resulting constitutive equation is then used for further numerical calculations.

Kurzfassung

Das Dämpfungsverhalten von Strukturen wird wesentlich beeinflusst von den dissipativen Eigenschaften seiner Fügestellen sowie dem Dämpfungsvermögen der verwendeten Werkstoffe. Blatt 2 der VDI-Richtlinie Werkstoff- und Bauteildämpfung VDI 3830 widmet sich der Modellierung von linearer und nicht-linearer Werkstoffdämpfung, während in Blatt 5 verschiedene experimentelle Techniken zur Gewinnung geeigneter Kennwerte zusammengestellt sind. Der vorliegende Beitrag gibt einen Überblick über die Phänomene linear-viskoelastischen Materialverhaltens und ihre Modellierung mit ganzzahligen Zeitableitungen sowie deren Erweiterung mit Hilfe von fraktionalen Zeitableitungen.

Am Beispiel eines technischen Kunststoffs wird die Ermittlung von Materialparametern aus verschiedenen Versuchen dargelegt, die einen größeren Frequenz- und Temperaturbereich abdecken. Auf der Basis von thermorheologisch einfachem Materialverhalten lässt sich daraus eine 'Master-Kurve' identifizieren, durch die das Werkstoffverhalten über einen extrem großen Frequenzbereich abgebildet wird. Die Modellierung der so gewonnenen Werkstoffeigenschaften wird mit dem Konzept der fraktionalen Ableitungen auf elegante Art mit wenigen Materialparametern gelöst und weitergehenden numerischen Berechnungen zugänglich gemacht.

1 Introduction

The calculation of the dynamic behavior of any structure requires knowledge about its stiffness and its mass distribution. In addition, if energy dissipation cannot be neglected, the damping properties of the structure also have to be modeled. Measurements of the stiffness and the mass properties of engineering materials and their inclusion into any numerical calculation method such as the Finite Difference Method (FDM), the Finite Element Method (FEM), or the Boundary Element Method (BEM) does not present any serious difficulties. In contrast, the determination of the dissipative properties of materials and assembled structures is a difficult task, especially if the amount of damping is low compared to the deformation energy and the kinetic energy of the structure under consideration. Moreover, the current techniques for modeling damping are in many cases insufficient.

In any experimental setup for the measurement of material damping, some amount of energy is lost through the mounting or suspension of the material sample or through air friction. Such losses will be misinterpreted as material damping losses and thus falsify the results, especially for low-damping materials. Also, the amount of damping depends on the frequency, the amplitude, or the temperature. Such dependencies are particulary evident in the case of rubber materials and plastics [17, 19]. The detection of joint damping depends on even more parameters such as the materials involved, their surface texture and contact pressure, the amplitude of the exciting force, interface layers, etc.

Hence, the modeling of damping behavior is a demanding task. A simple approach can be made by an experimental modal analysis of the structure under consideration, which yields its modal shapes and the corresponding modal damping factors. A numerical model then might be set up based on the real mode shapes of the undamped system and the measured modal damping values. However, This approach does not allow numerical prediction of the structure's damping properties. In addition, the damping behavior is only valid for the structure under consideration and cannot be transferred to any other structure. The overall damping behavior can be interpreted as an integral result of many distinct damping mechanisms, whereby the individual loss mechanisms are not understood.

Thus, for a systematic approach one has to investigate and to model the different contributions to the overall damping behavior separately. This will result in local damping models for the different materials and joint regions. Local modeling of damping leads to complex eigenmodes which can also be observed in experimental investigations. Due to the complexity of the matter several research projects have been initiated to address different aspects of the underlying physics, to perform experimental investigations, and to develop adequate damping models.

As long as a material or a complete structure is operated within its linear range or can be

linearized about an operation point, linear viscoelastic models are used to describe the structure's damping properties [17]. One advantage of this approach is the possibility to carry out calculations both in the time domain and in the frequency domain. In addition, results from an (also linear) experimental modal analysis can directly be linked to numerical approaches.

Linear viscoelastic constitutive equations can be written most generally in terms of hereditary integrals [7, 19]. In this formulation, the so-called material functions — that is, the creep compliance or the relaxation function — are used to obtain a general stress-strain relation through use of the principle of superposition. Alternatively, linear viscoelasticity can be defined by a differential equation in time relating the stresses and strains and their temporal derivatives. A graphical representation of viscoelastic material behavior is obtained by a composition of springs and dashpots such as the Maxwell model, the Kelvin-Voigt model, or the Standard Linear Solid [32]. If one has to distinguish between the hydrostatic and the deviatoric material behavior, the respective constitutive equations have to be set up and treated separately [7].

Classical models of linear viscoelasticity predict a strong frequency dependence of the damping properties, whereas measurements on viscoelastic materials and joints reveal a very small change in their dissipative behavior with varying frequency [17, 19]. Thus, classical models have to be expanded to better concur with the measured data, which results in a high number of material parameters that have to be identified. Alternatively, the so-called model of constant hysteresis might be used in frequency-domain calculations. However, this model leads to non-causal material behavior in the time domain [10].

A better approximation is obtained by the use of fractional time derivatives [17]. These 'fractional models' have been verified to fulfill the second law of thermodynamics and show causal material behavior [20]. Thus, they can be used in time domain and in frequency domain calculations. The appearance of fractional derivatives in viscoelastic constitutive equations is physically sound [24, 8, 33] and leads to models that concur well with the measured data over broad ranges of time or frequency with few material parameters [17]. This concept was first suggested by Gemant [13, 14] in 1936 and had its revival by the research of Bagley and Torvik [2, 4, 3, 29] in the beginning of the 1980s. Applications of fractional derivatives in very different disciplines such as viscoelasticity, control theory, diffusion processes, biophysics, or thermodynamics are subject matters of recent research projects [16, 21, 23].

2 Classical Models of Linear Viscoelasticity

Classical linear viscoelastic material models can be represented by an arbitrary composition of springs and dashpots where the stresses σ in the springs are proportional to their strains ε

$$\sigma = E\varepsilon \tag{1}$$

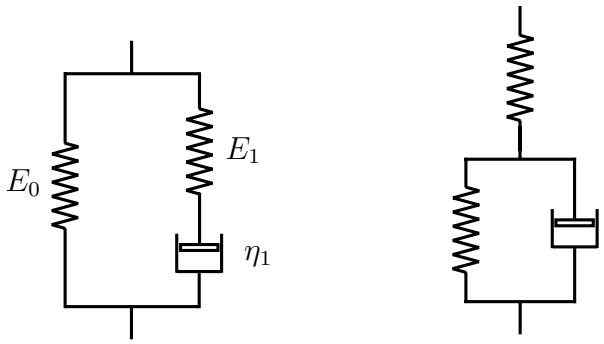

Figure 1: The 3-parameter model: two equivalent representations

and the stresses σ of the dashpots proportional to their strain rates ε

$$\sigma = \eta\dot{\varepsilon}\,. \tag{2}$$

The simplest model for solids that is able to show all phenomena related to viscoelasticity is the 3-parameter model (also called 'standard linear solid' or 'Zener model'), see Fig. 1. It consists of a spring (E_0) in parallel to a Maxwell element (E_1, η_1) and degenerates to a Kelvin element for $E_1 \to \infty$. Its constitutive equation is given by

$$\sigma + \frac{\eta_1}{E_1}\,\dot{\sigma} = E_0\varepsilon + \eta_1\,\frac{E_0 + E_1}{E_1}\,\dot{\varepsilon}\,. \tag{3}$$

Regarding the definition of viscoelasticity by means of hereditary integrals, the relaxation function (i.e. the answer of the model to a single step in strain of amplitude $\hat{\varepsilon}$ at $t = 0$)

$$E(t) = \frac{\sigma(t)}{\hat{\varepsilon}} = E_0 + E_1\mathrm{e}^{-t/\tau_\mathrm{R}}\,, \quad t > 0 \tag{4}$$

can be derived from Eq. (3). In Eq. (5) $\tau_\mathrm{R} = \eta_1/E_1$ denotes the relaxation time. Alternatively, the creep compliance (i.e. the answer of the model to a single step in stress of amplitude $\hat{\sigma}$ at $t = 0$)

$$J(t) = \frac{\varepsilon(t)}{\hat{\sigma}} = \frac{1}{E_0} - \frac{E_1}{E_0(E_0 + E_1)}\mathrm{e}^{-t/\tau_\mathrm{C}}\,, \quad t > 0 \tag{5}$$

is found from Eq. (3), where $\tau_\mathrm{C} = \eta_1(E_0 + E_1)/(E_0E_1)$ is called the retardation time. Using the principle of superposition, the answer of the model to an arbitrary load can be found as [32]

$$\sigma(t) = \varepsilon(t)E(0) + \int_0^t \varepsilon(\tau)\dot{E}(t-\tau)\,\mathrm{d}\tau \tag{6}$$

or

$$\varepsilon(t) = \sigma(t)J(0) + \int_0^t \sigma(\tau)\dot{J}(t-\tau)\,\mathrm{d}\tau\,. \tag{7}$$

Transferring Eq. (3) into the frequency domain yields

$$\tilde{\sigma} = \frac{E_0 + \mathrm{i}\,\eta_1\omega\,\frac{E_0+E_1}{E_1}}{1 + \mathrm{i}\,\frac{\eta_1\omega}{E_1}}\,\tilde{\varepsilon} = E^*\tilde{\varepsilon} \tag{8}$$

where a tilde denotes the Fourier transformed and the abbreviation

$$E^* = E' + \mathrm{i}E'' = (1 + \mathrm{i}\eta)E' \tag{9}$$

is called the complex modulus. The latter consists of the storage modulus E' and the loss modulus E'' and can alternatively be written in terms of the loss factor η. For the 3-parameter model one obtains

$$E' = \frac{E_0 + (\eta_1\omega)^2\,\frac{E_0+E_1}{E_1^2}}{1 + \left(\frac{\eta_1\omega}{E_1}\right)^2}\,, \qquad\qquad E'' = \frac{\omega\eta_1}{1 + \left(\frac{\eta_1\omega}{E_1}\right)^2}\,. \tag{10}$$

The time- and the frequency-dependent properties of the 3-parameter model are displayed in Fig. 2 on half-logarithmic scales. By adjusting the free parameters one can control the respective magnitudes and relaxation or retardation times of the curves. But all curves will only be 'active' within approximately two decades in time or frequency. Since most materials or joint patches show a weak frequency dependence that typically covers a range of several decades, in classical viscoelasticity models are used that consist of many spring/dashpot combinations as displayed in Fig. 3. The resulting constitutive equations can be written in the form

$$\sum_{k=0}^{n} p_k \mathrm{D}^k\sigma = \sum_{k=0}^{m} q_k \mathrm{D}^k\varepsilon\,, \tag{11}$$

where the operator D^k denotes the derivative of order k with respect to time and p_k, q_k are the material-dependent coefficients. In viscoelastic models according to Fig. 3 the number $m = n$ equals the number of Maxwell elements (spring-dashpot combinations connected in series) or the number of Kelvin-Voigt elements (spring-dashpot combinations in parallel), respectively. The relaxation function and the creep function are deduced by means of a Laplace transformation [32] and can be written in the form

$$E(t) = E_0 + E_1\mathrm{e}^{-t/\tau_{R_1}} + E_2\mathrm{e}^{-t/\tau_{R_2}} + \ldots + E_n\mathrm{e}^{-t/\tau_{R_n}} \tag{12}$$

$$J(t) = J_0 + J_1\mathrm{e}^{-t/\tau_{C_1}} + J_2\mathrm{e}^{-t/\tau_{C_2}} + \ldots + J_n\mathrm{e}^{-t/\tau_{C_n}}\,, \tag{13}$$

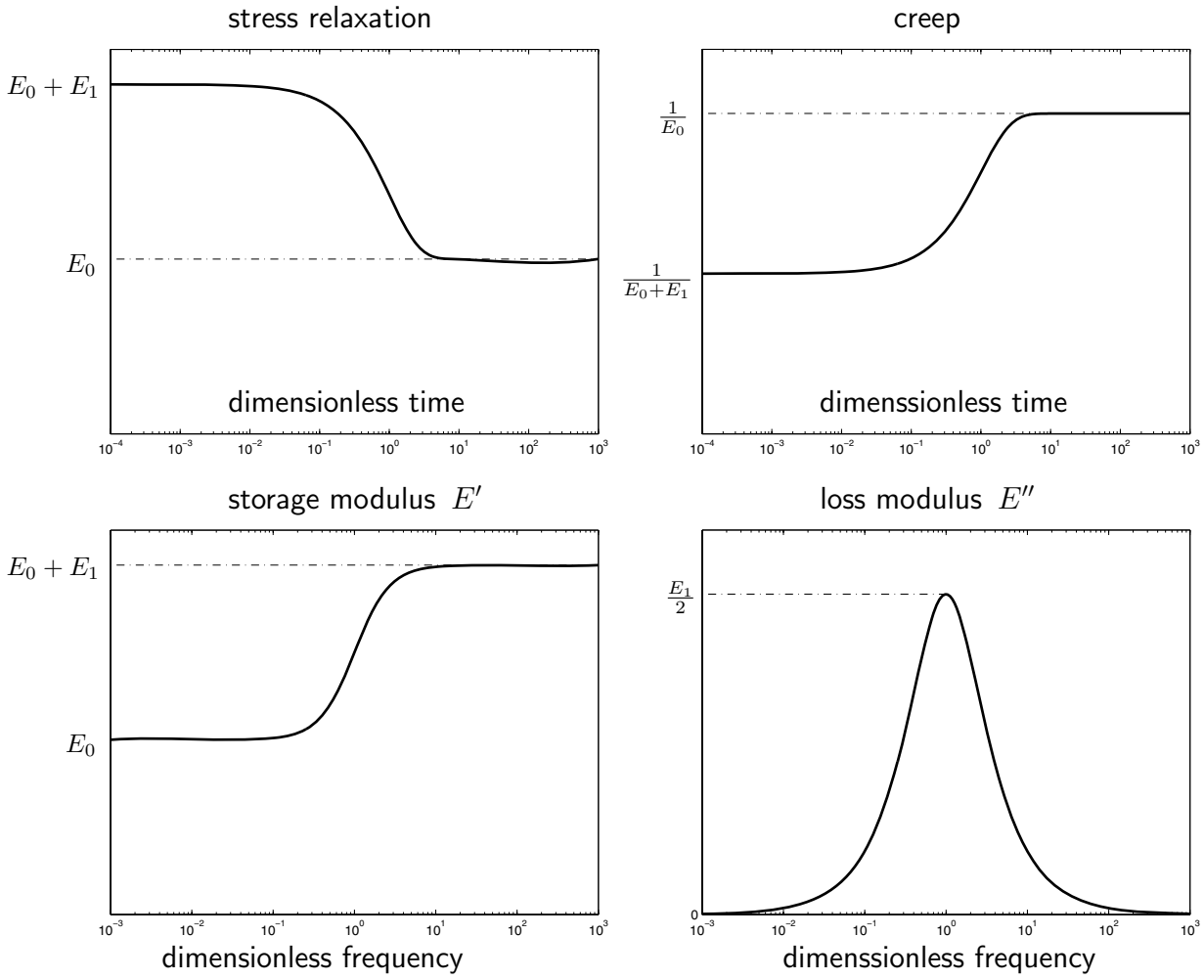

Figure 2: Time- and frequency-dependent behavior of the 3-parameter model

where τ_{C_i} and τ_{R_i} are the different creep and relaxation times, respectively. The frequency-domain representation of Eq. (11) results in

$$\tilde{\sigma} = \frac{\sum_{k=0}^{m} q_k (\mathrm{i}\omega)^k}{\sum_{k=0}^{n} p_k (\mathrm{i}\omega)^k} \, \tilde{\varepsilon} = E^* \tilde{\varepsilon} \, . \tag{14}$$

The respective time- and frequency-dependent constitutive behavior is depicted in Fig. 4. The resulting curves can be interpreted as a superposition of n curves as they are obtained from the 3-parameter model, see Fig. 2. Thus, the curves still show a strong frequency dependency that now covers a broader range of time and frequency at the expense of an increasing number of material parameters. In practice, commonly one Maxwell element is added for each decade in time or frequency to be covered as a compromise between the objectionable overshooting behavior and an increasing number of material parameters. An example is given in Section 5.

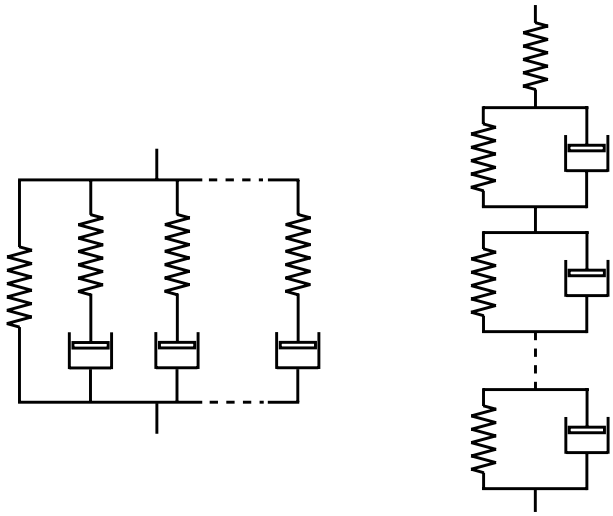

Figure 3: The n-parameter model: two equivalent representations

3 Fractional Models of Linear Viscoelasticity

A generalization of classical viscoelastic models is obtained by the use of fractional derivatives instead of integer-order derivatives. A fractional derivative of order α of a function $f(t)$ with respect to time is given by (Riemann-Liouville definition, see e.g. [21, 23])

$$ {}_a\mathrm{D}_t^{\alpha} f(t) = \mathrm{D}^n \left[{}_a\mathrm{D}_t^{\alpha-n} f(t) \right] = \frac{1}{\Gamma(n-\alpha)} \mathrm{D}^n \left[\int_a^t \frac{f(\tau)}{(t-\tau)^{\alpha+1-n}} \, \mathrm{d}\tau \right] , \qquad n \in \mathbb{N},\, \alpha \in \mathbb{R},\, n > \alpha \, , \tag{15} $$

where

$$ \Gamma(x) = \int_0^{\infty} y^{x-1} \mathrm{e}^{-y} \, \mathrm{d}y \tag{16} $$

is the Gamma function [1]. Eq. (15) provides the classical derivatives for $\alpha \in \mathbb{N}$. Note that in contrast to integer-order derivatives a fractional derivative is a non-local operator since the history of the function in the interval $[a, t]$ contributes to its actual value, similar to an integration. The question of what value has to be taken for the lower boundary a depends on the physical interpretation of the underlying problem. In general, the lower boundary (also called 'terminal') is set to $a = -\infty$. The Fourier transformation of a fractional derivative of a function $f(t)$ leads to

$$ \mathcal{F} \left[{}_{-\infty}\mathrm{D}_t^{\alpha} f(t) \right] = (\mathrm{i}\omega)^{\alpha} \tilde{f} \, , \tag{17} $$

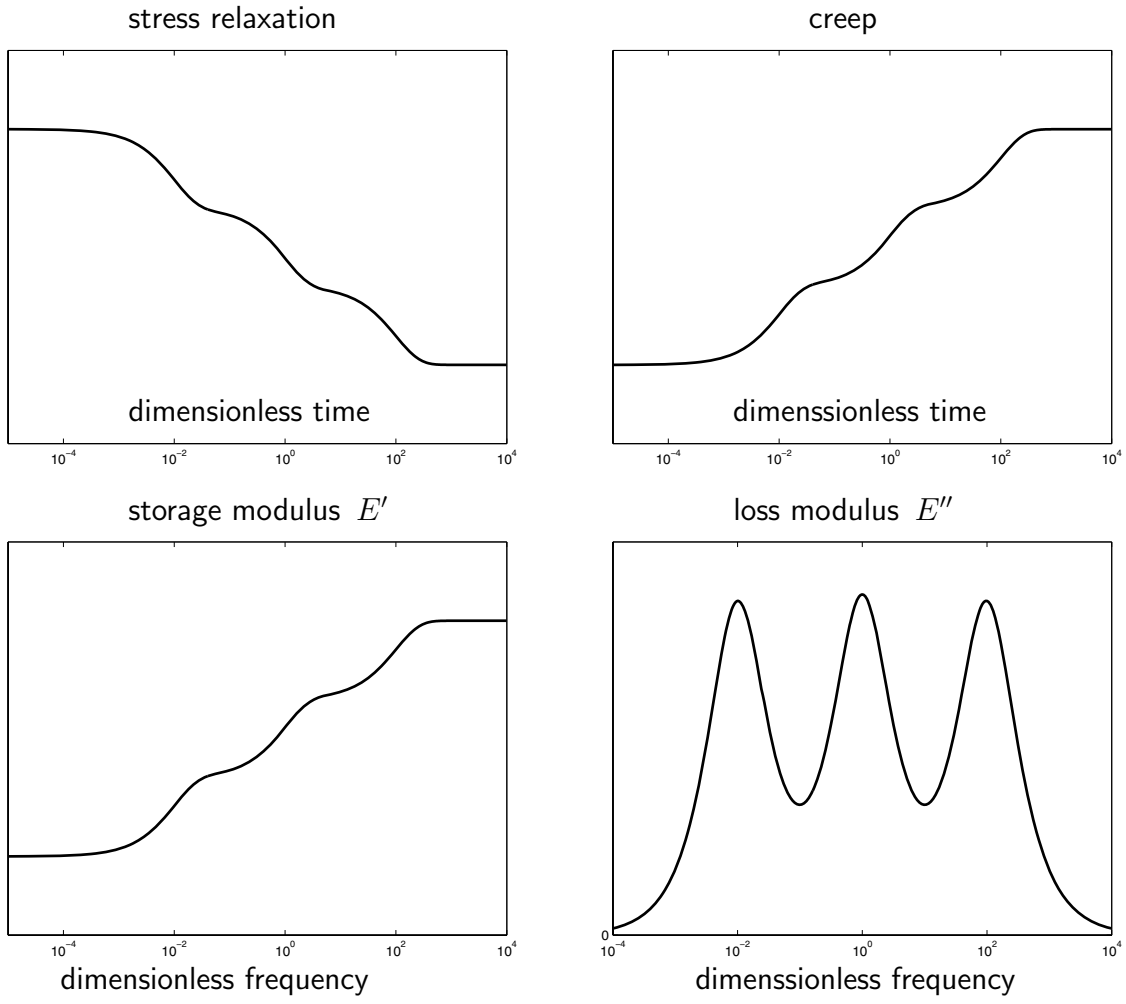

Figure 4: Time- and frequency-dependent behavior of the n-parameter model (for n=7)

where $\tilde{f}$ is the Fourier transformed of the function f. This essential property can also be used to *define* a fractional derivative [5].

In order to become more familiar with fractional derivatives, some examples are given in the following. The fractional derivative of an exponential function (see [21])

$$ {}_{-\infty}\mathrm{D}_t^{\alpha} \exp(ct) = c^{\alpha} \exp(ct) \tag{18} $$

also results in an exponential function and for trigonometric functions it can be shown that [25]

$$ {}_{-\infty}\mathrm{D}_t^{\alpha} \sin(ct) = c^{\alpha} \sin\left(ct + \alpha \frac{\pi}{2}\right) , \tag{19} $$

$$ {}_{-\infty}\mathrm{D}_t^{\alpha} \cos(ct) = c^{\alpha} \cos\left(ct + \alpha \frac{\pi}{2}\right) . \tag{20} $$

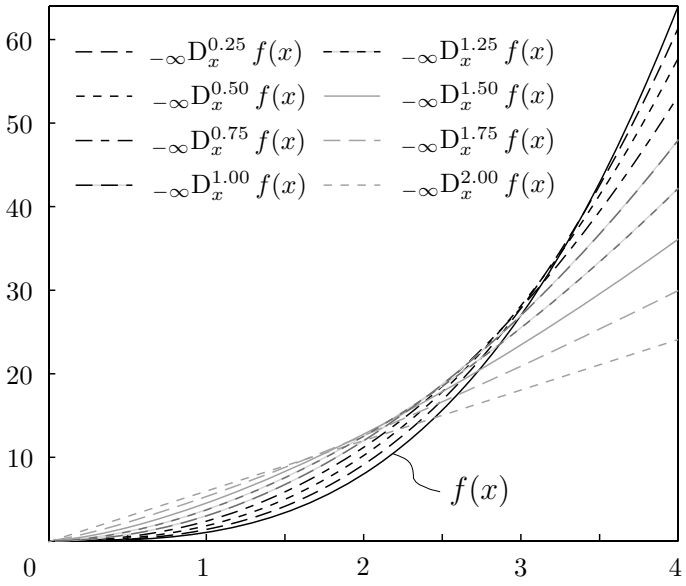

Figure 5: Function $f(t)$ and its fractional derivatives of order $\alpha = 1/4,\, 2/4,\, 3/4,\, \ldots,\, 8/4$

Finally, in Fig. 5 the function

$$f(x) = \begin{cases} x^3 & \text{for} \quad x \geq 0 \\ 0 & \text{for} \quad x < 0 \end{cases} \tag{21}$$

and its fractional derivatives in steps of $1/4$ including the first-order and the second-order derivatives are displayed.

So-called 'fractional constitutive equations' can be derived by replacing the integer-order derivatives in Eq. (11) by fractional derivatives resulting in

$$\sum_{i=0}^{n} p_i \, {}_{-\infty}\mathrm{D}_t^{\alpha_i} \sigma = \sum_{i=0}^{m} q_i \, {}_{-\infty}\mathrm{D}_t^{\beta_i} \varepsilon \, . \tag{22}$$

In Eq. (22) the values of α_i and β_i are additional free parameters that can be adjusted to meet the measured data. A drawback of this approach is that additional conditions have to be fulfilled to guarantee a constitutive behavior of a solid (limited flow) and to ensure the capability for a jump in strain. Moreover, restrictions on the parameters to ensure purely dissipative behavior (i.e. to fulfill the second law of thermodynamics) for a general model as described in Eq. (22) are not available.

An alternative way to deduce fractional constitutive equations makes use of a generalized damping element that is also called a 'fractional element' or a 'spring-pot' [18]

$$\sigma = p \, {}_{-\infty}\mathrm{D}_t^{\alpha} \, \varepsilon \, . \tag{23}$$

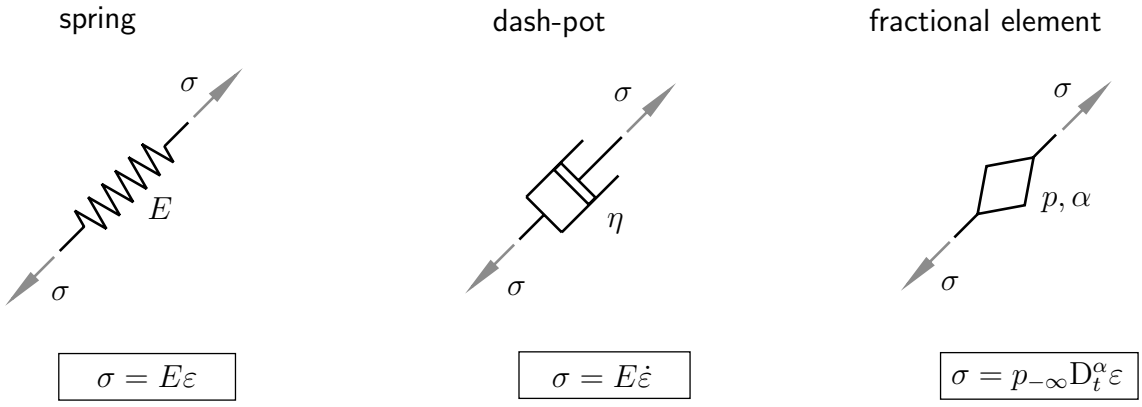

Figure 6: Illustration of the generalized 'fractional' element

A fractional element usually is illustrated as a diamond and possesses two free parameters p and α, see Fig.6. For $\alpha = 1$ Eq. (23) switches over to the constitutive equation of a dashpot (2) where p becomes the meaning of a viscosity η and for $\alpha = 0$ Eq. (23) is identical to the constitutive equation of a spring (1) where p is equivalent to Young's modulus E. The capabilities of a solid are assured by simply replacing the dashpots of a respective classical model by fractional elements. In case of the classical 3-parameter model one arrives at the 'fractional 3-parameter model' and its constitutive equation

$$\sigma + \frac{p}{E_1}\,{}_{-\infty}\mathrm{D}_t^{\alpha}\sigma = E_0\varepsilon + p\,\frac{E_0+E_1}{E_1}\,{}_{-\infty}\mathrm{D}_t^{\alpha}\varepsilon\,. \tag{24}$$

Using relation (17), the constitutive equation (24) can be transformed into the frequency domain

$$\tilde{\sigma} = \frac{E_0 + (\mathrm{i}\omega)^{\alpha}\, p\, \frac{E_0+E_1}{E_1}}{1 + (\mathrm{i}\omega)^{\alpha}\, \frac{p}{E_1}}\,\tilde{\varepsilon} = E^*\tilde{\varepsilon}\,. \tag{25}$$

From Eqns. (17) and (25) it becomes obvious that the frequency dependence of the model's properties is directly linked to the order of derivative α and becomes weaker for decreasing α.

Regarding the hereditary integral formulation, the relaxation function $E(t)$ or the creep compliance $J(t)$ have to be calculated from the constitutive equation (24). This has been done by Caputo and Mainardi [6] and leads to

$$E(t) = E_0 + E_1\,\mathcal{E}_{\alpha}\left(-\frac{E_1}{p}t^{\alpha}\right) \tag{26}$$

$$J(t) = \frac{1}{E_0} - \frac{E_1}{E_0(E_0+E_1)}\,\mathcal{E}_{\alpha}\left(-\frac{E_0E_1}{p(E_0+E_1)}t^{\alpha}\right) \tag{27}$$

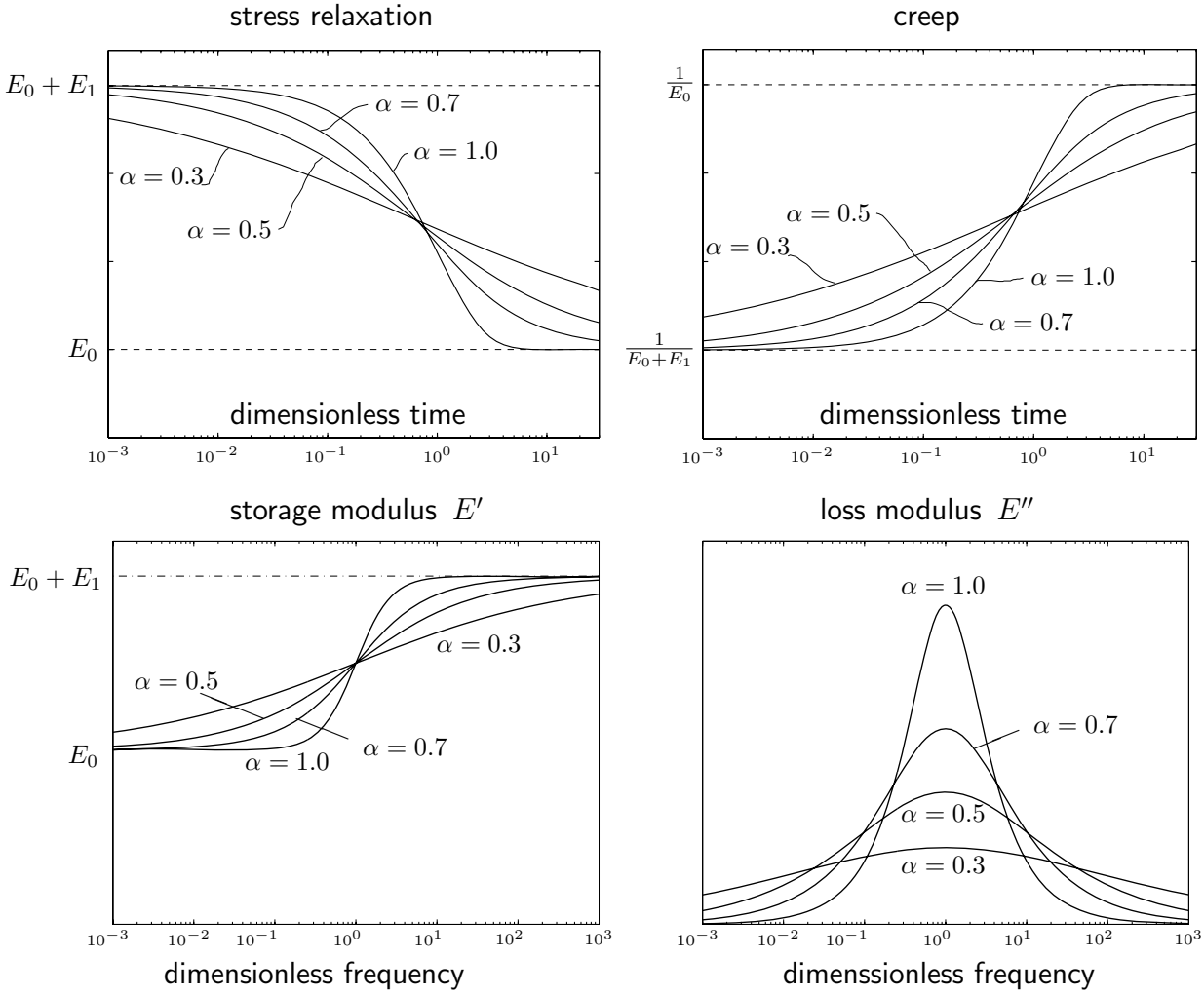

Figure 7: Time- and frequency-dependent behavior of the n-parameter model (for n=7)

where

$$\mathcal{E}_\alpha(x) = \sum_{k=0}^{\infty} \frac{x^k}{\Gamma(\alpha k + 1)} \tag{28}$$

is the Mittag-Leffler function which can be interpreted as a generalized exponential function. The influence of the order of derivative α on the material functions is depicted in Fig. 7. Similar to the frequency dependence, the time dependence is reduced with decreasing α and leads to a smoother changeover from the initial values to the long-term properties.

Any fractional viscoelastic model made up by an arbitrary composition of springs, dashpots, and fractional elements is proved to exhibit causal behavior and to fulfill the second law of thermodynamics [20]. Moreover, the appearance of fractional derivatives in the constitutive equations of viscoelastic media was already deduced on the basis of molecular theories in the 1950s [24, 8, 33].

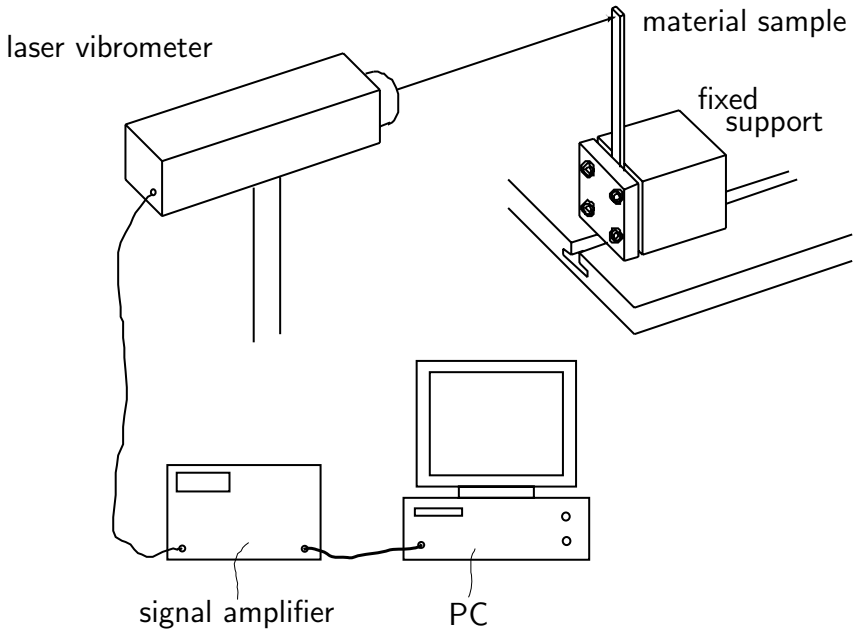

Figure 8: Experimental setup for the measurement of decaying free vibrations

4 Experimental investigations

As an example, the engineering plastic Delrin^{TM} 100 manufactured by DuPont company is considered. Delrin^{TM} is a thermoplastic polyoxymethylene (POM) that is widely used in technical applications (e.g. as zippers or gears) due to its relatively high stiffness combined with a low friction coefficient.

Two different experiments are performed in order to obtain the frequency-dependent complex modulus. At first, free decay experiments (cf [31]) are carried out with cantilevers made of Delrin. The samples are fixed at one end and excited to perform free oscillations that are measured by a laser vibrometer, see Fig. 8. Different frequencies are obtained by a modification of the free length ℓ and the use of samples of different thickness.

For purely elastic materials the first eigenfrequency is given by [15]

$$\omega_0 = \left(\frac{1,875}{\ell}\right)^2 \sqrt{\frac{EI}{\rho A}}\,. \tag{29}$$

Since the material is weakly damped, the measured eigenfrequency ω is nearly identical to the undamped frequency ω_0 and real part of the complex modulus

$$E' \approx E \tag{30}$$

is good approximation equal to Young's modulus E which can be calculated from Eq. (29). The complex part E'' of the complex modulus is found from the decay behavior of the

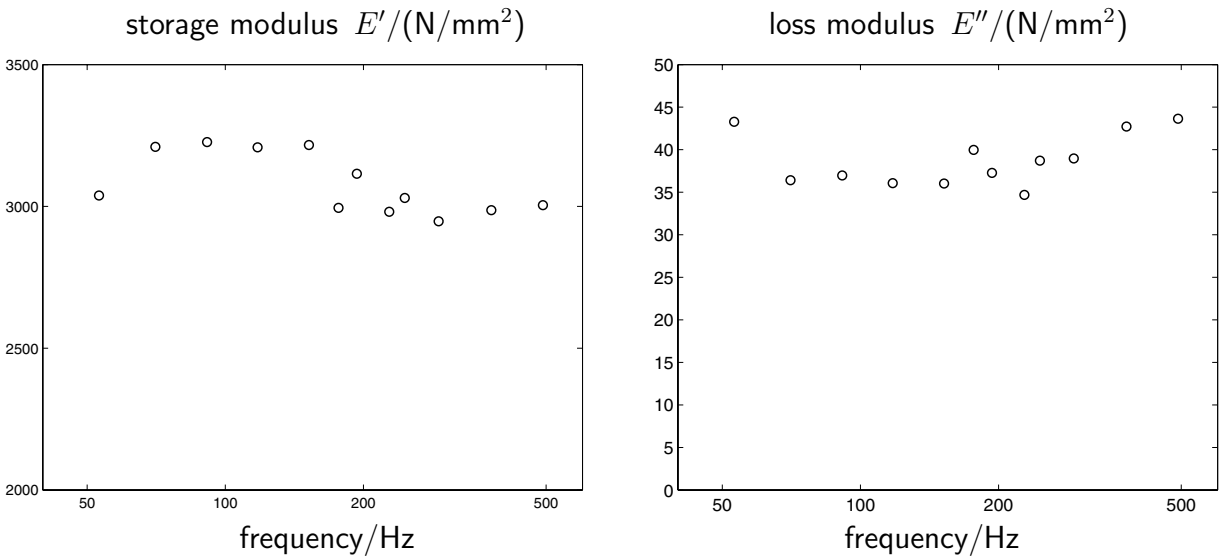

Figure 9: Storage modulus and loss modulus detected from free decay experiment

oscillation. The envelope $x_\mathrm{e}(t)$ of the oscillation can be expressed as

$$x_\mathrm{e}(t) = \hat{x}\exp(-\xi\omega_0 t)\,, \tag{31}$$

where the damping ratio ξ is found from a parameter identification. Finally, the loss modulus can be calculated [31]

$$E'' \approx 2\xi E'\,. \tag{32}$$

The results of this experiment cover a range from 50 Hz up to 500 Hz and are depicted in Fig. 9.

The second set of experiment is performed by a testing machine RMS-800/RDSII (Rheometrics) in which a sample is subjected to rotational deformations

$$\phi(t) = \hat{\phi}\sin(\omega t) \tag{33}$$

and the resulting torque is measured. Since the sample's dimensions are known, the shear stresses τ and the shear strains ε

$$\tau(t) = \hat{\tau}\sin(\omega t) \tag{34}$$

$$\varepsilon(t) = \hat{\varepsilon}\sin(\omega t - \Phi_0) \tag{35}$$

can be calculated. Again, for weakly damped materials the imaginary part of the shear modulus is given by

$$G' \approx \frac{\hat{\varepsilon}}{\hat{\tau}} \tag{36}$$

and the loss modulus is linked to the phase angle Φ_0 [30]

$$G'' = \tan \Phi_0 \, G' \, . \tag{37}$$

The testing machine allows to perform measurements at different temperatures and frequencies. For the material under consideration measurements are accomplished within a temperature range from $-20°\mathrm{C}$ up to $50°\mathrm{C}$ in steps of $2°\mathrm{C}$ each of which including the frequencies 1 Hz, 2 Hz, 5 Hz, 10 Hz, 20 Hz and 50 Hz.

Assuming thermo-rheological simple material behavior, a shift in temperature corresponds to a shift in frequency and vice versa. Thus, a so-called master curve can be determined, that covers a broad range of frequencies f at one reference temperature T_0 .

The complex modulus at one distinct frequency f_1 and reference temperature T_0 is equal to the complex modulus at some other temperature T_2 and a frequency f_2 , where a function γ can be found that 'scales' the frequency f_2 to f_1 :

$$G^*(f_1, T_0) = G^*(f_2 \gamma(T_2, T_0), T_0) \, . \tag{38}$$

Once the temperature-dependent function $\gamma(T, T_0)$ for a viscoelastic material is identified, measurements at any temperature can be 'converted' into a so-called reduced frequency at the reference temperature T_0 [17]. This results in the master curve one is looking for. If storage and loss modulus are unique functions of the reduced frequency $f\gamma(T, T_0)$ they must be unique functions of each other. This can be checked by the so-called 'wicket plot' where the loss factor η (cf Eq. (9)) of the measured data is plotted against the storage modulus. As long as all data points lie close to one curve, the requirements for thermo-rheological simplicity are fulfilled. Considering the measurements made with Delrin$^{\mathsf{TM}}$, the data for 20 Hz and for 50 Hz are skipped since the corresponding loss factors obviously are connected to some systematic error. The resulting data shows good agreement with the requirement for thermo-rheological simple material behavior, see Fig. 10.

In practice, since the a pair f_2, T_2 that exactly matches the reference value $G^*(f_1, T_0)$ generally will not be found, the measurements at a different temperature are shifted in frequency to match the data at some overlapping area. This can be seen from Fig. 11 for the material under consideration. The frequency-shift function $\gamma(T_2, T_0)$ can either be defined by identifying individual shift factors

$$\gamma_2(T_2, T_0) \, , \quad \gamma_3(T_3, T_0) \, , \quad \gamma_4(T_4, T_0) \, , \ldots \tag{39}$$

of all temperatures at which measurements are made. Alternatively some analytical function can be set up, where the most common approaches are given by the Williams-Landel-Ferry (WLF) relationship

$$\log \left[\gamma(T_2, T_0) \right] = -c \, \frac{T - T_0}{b + T - T_0} \tag{40}$$

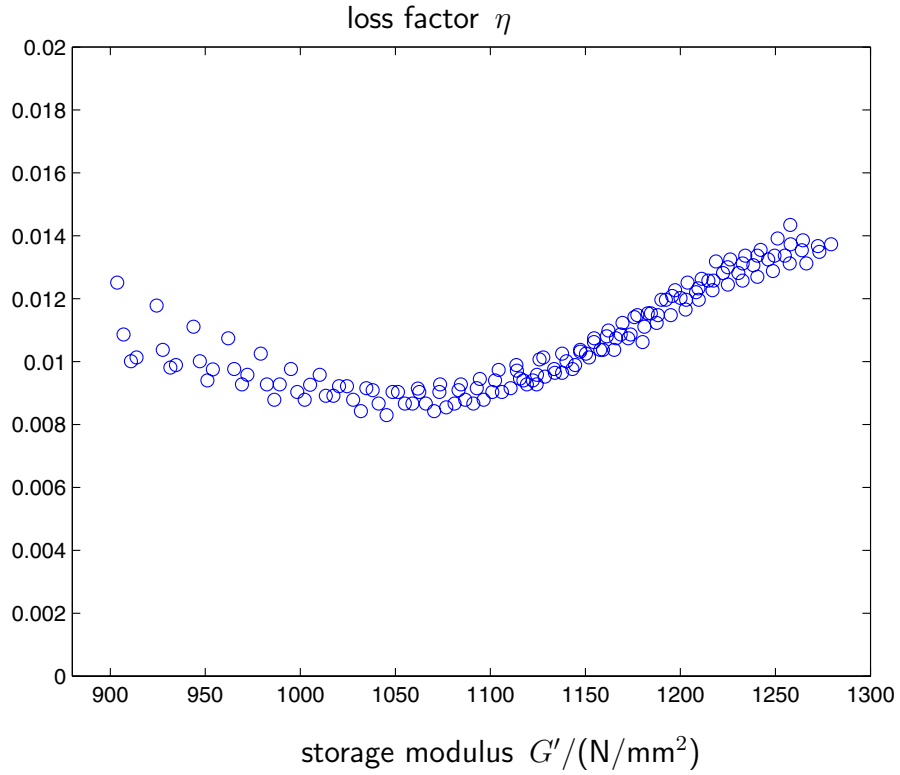

Figure 10: Wicket plot for the measured data of Delrin™

and the Arrhenius shift factor equation

$$\log\left[\gamma(T_2, T_0)\right] = T_\mathrm{A}\left(\frac{1}{T} - \frac{1}{T_0}\right), \tag{41}$$

where the free parameters b, c and T_A have to be identified, respectively.

For the measured complex modulus of Delrin™ linear interpolation in the half-logarithmic scale was used to identify the individual shift factors for the 36 different temperatures using $T_0 = 0°\mathrm{C}$ as reference temperature. The result can be seen from Fig 11. Especially for the storage modulus a unique curve is obtained even though for low frequencies smaller than $10^{-15}\,\mathrm{Hz}$ there is no overlapping of the shifted frequencies any more.

Both measurements can now be used to check for consistency and to determine Poisson's ratio ν from the relationship

$$G = \frac{E}{2(1+\nu)}. \tag{42}$$

Since the measurement of the loss modulus always is associated with some uncertainties, either the storage modulus or the amplitudes of the complex modulus can be used in Eq. (42). For Delrin™ , the Poisson's ratio

$$\nu \approx \frac{E}{2G} - 1 \approx 0.39 \tag{43}$$

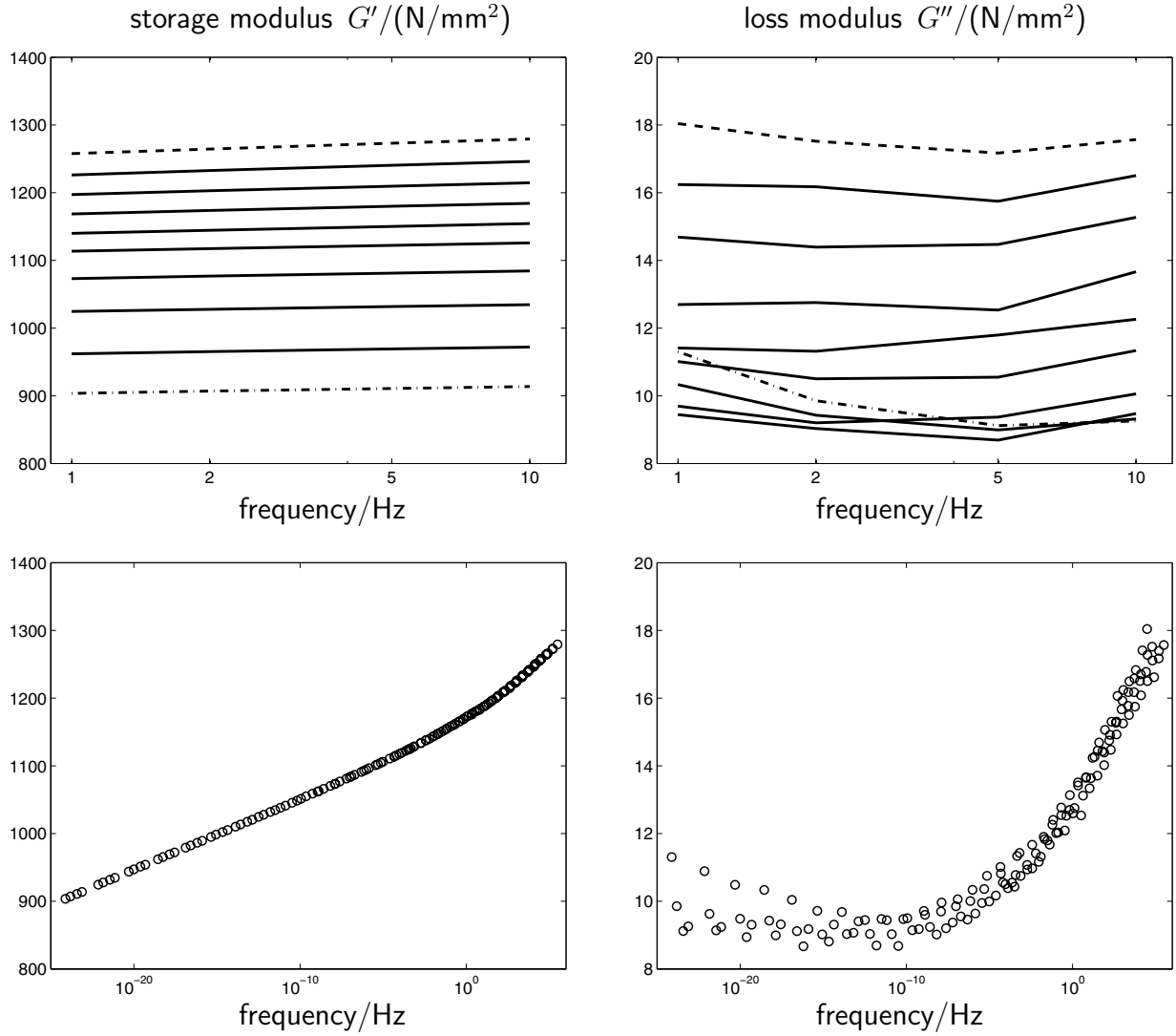

Figure 11: Temperature-dependent complex modulus as measured (top; dashed: lowest temp. ($-20°$C), dash-dotted: highest temp ($50°$C)) and resulting master curve at $0°$C (below)

is detected from the measured storage modulus, where both measurements are carried out at a temperature of $T = 22°\mathrm{C}$. The resulting data is depicted in Fig. 12. Since both, the storage modulus and the loss modulus of the measurements are in good agreement with a Poisson's ratio $0 < \nu = 0.39 < 0.5$, the two measurements are verified.

Generally speaking, Poisson's ratio $\nu(f, T)$ is a function of the frequency f and the temperature T. However, since the dependency on f and T has shown to be slight and is difficult to measure whereas its influence on a structure's behavior is marginal, a frequency-independent Poisson's ratio is often assumed.

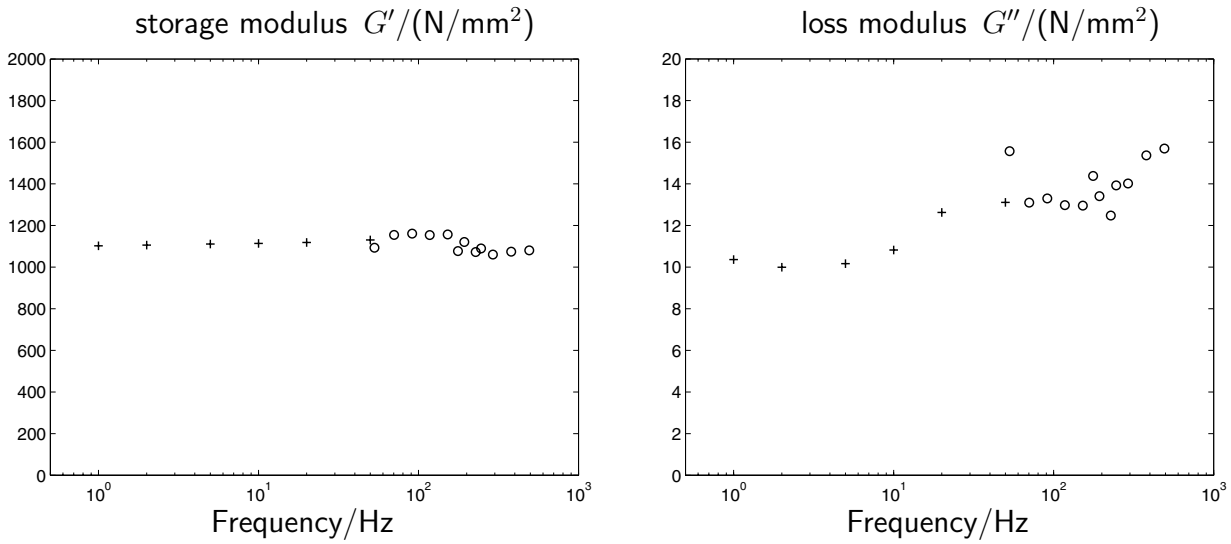

Figure 12: Frequency-dependent complex modulus for Delrin$^{\mathrm{TM}}$ at $22°\mathrm{C}$. $+$: measurements with testing machine o: free decay experiments

5 Parameter identification

The complex modulus obtained from the experiments covers a range of approximately 30 decades in frequency. Following the 'rule' from practical experience with classical models which states that one Maxwell element is necessary per decade, a model consisting of 30 Maxwell elements (i.e. 61 free parameters) has to be identified. This is done by means of a least-squares fit where the residuum R to be minimized is given by

$$R = \sum_{i=1}^{i_{\max}} \left[(G'_{i,\mathrm{measured}} - G'_{i,\mathrm{model}})^2 + w^2 \, (G''_{i,\mathrm{measured}} - G''_{i,\mathrm{model}})^2 \right] . \tag{44}$$

For the identification all available data points $i_{\max} = 36 \cdot 4 = 144$ are used. The residuum of the imaginary parts is weighted by a factor of w^2 where

$$w = \frac{G'_{\mathrm{max,measured}}}{G''_{\mathrm{max,measured}}} \tag{45}$$

is the proportion of the highest measured storage and loss modulus, respectively. The result displayed in Fig. 13 shows an extensive overshooting behavior associated with poor extrapolation properties.

In contrast, a fractional model depicted in Fig. 14 is identified using the same method, see Eq. (44). The model consists of 7 free parameters including the orders of derivatives α_1 and α_2. The identified parameters are given in Table 1. In comparison with the classical approach, the residuum is reduced by 42.4% whereas the fractional model requires only few parameters,

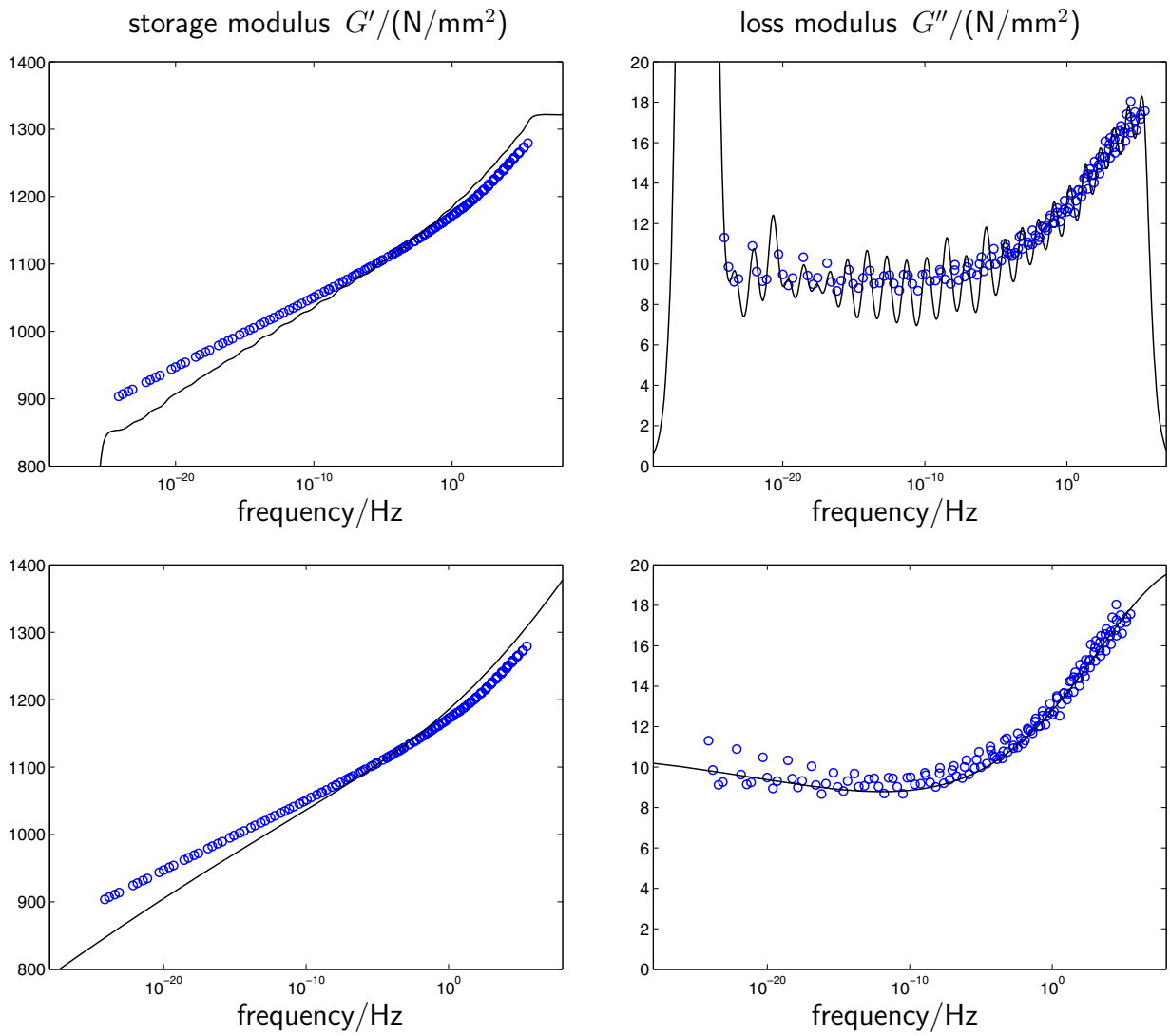

Figure 13: Parameter identification with a classical 61-parameter model (top) and a fractional 5-parameter model (bottom) o: measured values —: viscoelastic models.

does not show any overshooting behavior, and holds reasonable extrapolation properties, see Fig. 13. By a change of the weighting factor w, an improved fit to the storage modulus can be achieved at the expense of a reduced fit to the loss modulus. Similar properties of fractional models compared to the classical approach can be found from time-domain considerations of viscoelastic materials [26].

6 Example

The concept of fractional derivatives in linear viscoelasticity can be implemented into the Finite Difference Method (FDM) [28], the Boundary Element Method (BEM) [9, 11, 12], and the

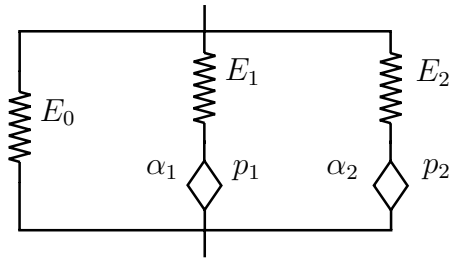

Figure 14: Fractional 5-parameter model

Table 1: Identified material parameters for shear deformation

$E_0/\frac{\mathrm{N}}{\mathrm{mm}^2}$	$E_1/\frac{\mathrm{N}}{\mathrm{mm}^2}$	$p_1/\frac{\mathrm{Ns}_1^\alpha}{\mathrm{mm}^2}$	α_1	$E_2/\frac{\mathrm{N}}{\mathrm{mm}^2}$	$p_2/\frac{\mathrm{Ns}_1^\alpha}{\mathrm{mm}^2}$	α_2
0.0	514.4	77.2	0.0794	1 324.2	7 198.5	0.0202

Finite Element Method (FEM) [22, 27] in the time domain and in the frequency domain. As an example, the dynamic response of a viscoelastic rod made of Delrin™ is calculated. For this purpose, the identified fractional viscoelastic model is converted from shear deformation to axial deformation according to Eq. (42), see Table 2. The rod is fixed at one end and subjected to a single step in load

$$F(t) = \begin{cases} 0 & \text{for } t \leq 0 \\ 100\,\mathrm{N} & \text{for } t > 0 \end{cases} \tag{46}$$

at its free end. The time-domain calculation is performed with the FDM where the discretization in time (Central Difference Method) and in space is of second-order accuracy, see [28]. The rod and its discretization are depicted in Fig. 15 where the total number of spatial nodes is $n = 30$. Since the length of the rod is $\ell = 2\,\mathrm{m}$, the nodal distance is given by $\Delta x \approx 68.97\,\mathrm{mm}$. The cross section of the rod is circular (diameter $d = 15\,\mathrm{mm}$) and the density of Delrin™ is $\rho = 1\,420\,\frac{\mathrm{kg}}{\mathrm{m}^3}$. The whole simulation time is $0.6\,\mathrm{s}$ were a time step size $\Delta t = 40\mu\mathrm{s}$ is used, resulting in $15\,000$ time steps.

The resulting deflection of the rod's free end is displayed in Fig. 16. Since the force $f(t)$ is acting during the whole simulation time, the decaying oscillation is superimposed by a creep

Table 2: Converted material parameters for axial deformation

$E_0/\frac{\mathrm{N}}{\mathrm{mm}^2}$	$E_1/\frac{\mathrm{N}}{\mathrm{mm}^2}$	$p_1/\frac{\mathrm{Ns}_1^\alpha}{\mathrm{mm}^2}$	α_1	$E_2/\frac{\mathrm{N}}{\mathrm{mm}^2}$	$p_2/\frac{\mathrm{Ns}_1^\alpha}{\mathrm{mm}^2}$	α_2
0.0	1 430.1	214.6	0.0794	3 681.3	20 011.8	0.0202

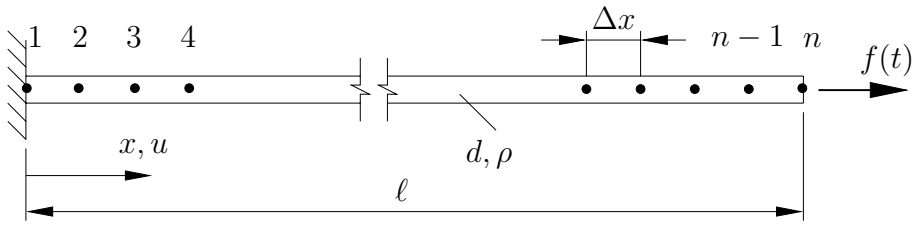

Figure 15: FDM discretization of the rod together with its boundary conditions

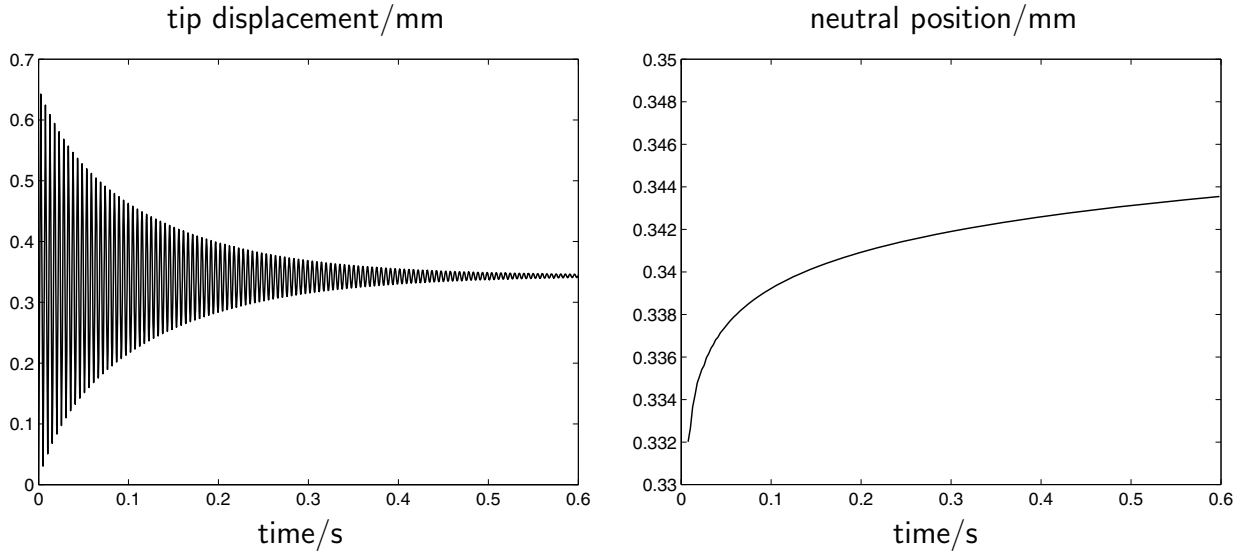

Figure 16: Decaying free oscillation of the rod's tip (left) and its neutral position (right)

process. The neutral position u_{np} can be calculated from the oscillating displacement signal using three successive extrema $u_{\mathrm{ex},1}$, $u_{\mathrm{ex},2}$, and $u_{\mathrm{ex},3}$

$$u_{\mathrm{np}} = \frac{u_{\mathrm{ex},1}u_{\mathrm{ex},3} - u_{\mathrm{ex},2}^2}{u_{\mathrm{ex},1} - 2u_{\mathrm{ex},2} + u_{\mathrm{ex},3}}\,. \tag{47}$$

The creep process detected from the calculated oscillation is also shown in Fig. 16.

A verification of the parameter identification and the implementation of the fractional constitutive equation into the FDM scheme can be achieved by detecting the complex modulus from the simulation's results. The first eigenfrequency f of a rod that is fixed at one end, see Fig. 15, is given by

$$f = \frac{c}{4\ell}\,, \tag{48}$$

where $c = \sqrt{E/\rho}$ is the speed of sound. The frequency $f = 194.1\,\mathrm{Hz}$ is identified from the calculated oscillation. Since the storage modulus is in very good approximation equal to

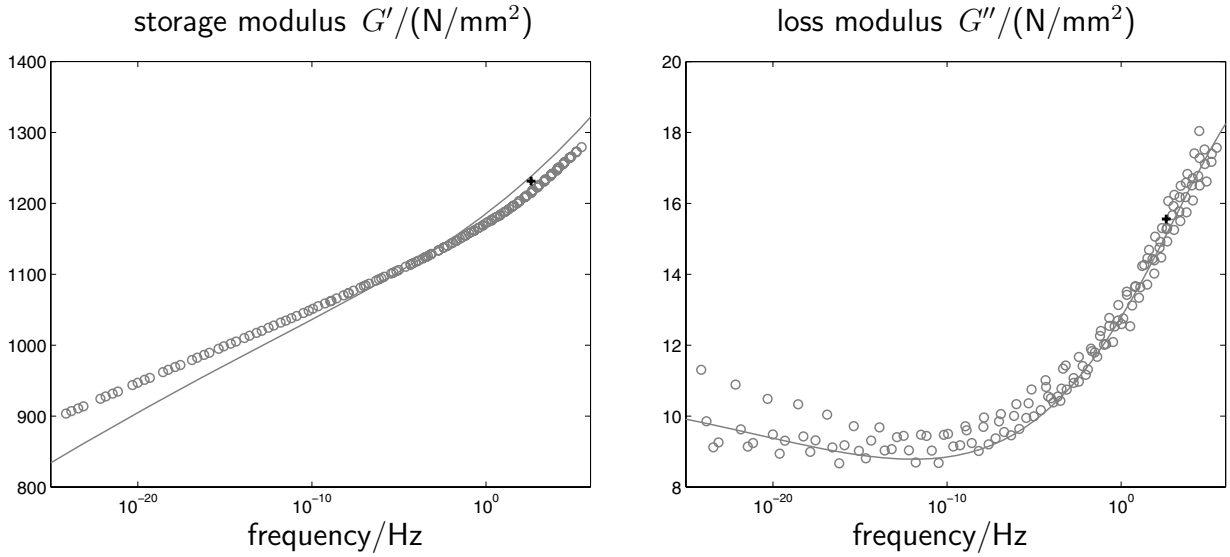

Figure 17: Comparison of the identified complex modulus from the calculation (+) with the measured data (o) and the fractional 5-parameter model (—)

Young's modulus E (cf. Section 4) one obtains

$$E' \approx E = 16\rho\ell^2 f^2 = 3\,423.4\,\frac{\mathrm{N}}{\mathrm{m}^2}\,. \tag{49}$$

The loss modulus is detected from the logarithmic decrement

$$\Lambda = \frac{1}{k}\ln\frac{\hat{x}_n}{\hat{x}_{n+k}} = 0.03970\,, \tag{50}$$

where the amplitudes $\hat{x}_n$ and $\hat{x}_{n+k}$ are the maxima after $n = 15$ and $n+k = 115$ oscillations with respect to the tip's neutral position. In so doing the first 14 oscillations are skipped to let the transients die out. This finally leads to (see [31])

$$E'' \approx 2\xi E' = \frac{\Lambda}{\pi}E' = 43.26\,\frac{\mathrm{N}}{\mathrm{m}^2}\,. \tag{51}$$

In order to compare the results with data from the experiments, see Fig. 17, the respective shear moduli

$$G' = \frac{E'}{2(1+\nu)} = 1\,231.4\,\frac{\mathrm{N}}{\mathrm{m}^2} \qquad\qquad G'' = \frac{E''}{2(1+\nu)} = 15.56\,\frac{\mathrm{N}}{\mathrm{m}^2} \tag{52}$$

are calculated. Since the results are in very good agreement with the measured data, the parameter identification and the numerical implementation are proven to be correct.

7 Summary

Linear viscoelastic constitutive equations are usually modeled by means of spring-dashpot combinations. Such models result in integer-order differential equations and exponential functions

as kernels in hereditary integral formulations for solid materials. This approach shows substantial deficiencies when measured material behavior has to be modeled over broad ranges of time or frequency. An alternative approach makes use of fractional derivatives where the order of derivative is interpreted as a free parameter that can become any real number. The curve-fitting properties of such models improve significantly while causal material behavior and thermo-mechanical consistency is assured. The models need only few parameters and can be implemented into numerical methods for structural calculations. As an example, an engineering plastic was investigated experimentally, and a master curve was deduced on the basis of thermo-rheologically simple material behavior. A classical and a fractional-derivative model were identified in order to highlight the advantages of the new approach. Finally, a numerical calculation of the dynamic response of a plastic rod was accomplished with the Finite Difference Method in the time domain. The results of the calculation were used to confirm the parameter identification and the numerical implementation of the fractional-derivative model.

8 Acknowledgments

The support of the project GA 209/25: 'Modellierung und Implementierung viskoelastischer Materialgesetze mit fraktionalen Zeitableitungen' by the Deutsche Forschungsgemeinschaft (DFG) which enabled us to perform these investigations is gratefully acknowledged. Also we would like to thank Nina Woicke for her support in performing the temperature-dependent measurements at the IKP, Universität Stuttgart.

References

[1] Abramowitz, M. ; Stegun, I. M.: *Pocketbook of Mathematical Functions*. Verlag Harri Deutsch, Frankfurt/M, 1984.

[2] Bagley, R. L. ; Torvik, P. J.: *A generalized derivative model for an elastomer damper*. Shock and Vibration Bulletin 49 (1979), S. 135–143.

[3] Bagley, R. L. ; Torvik, P. J.: *Fractional calculus — a different approach to the analysis of viscoelastically damped structures*. AIAA Journal 21 (1983), Nr. 5, S. 741–748.

[4] Bagley, R. L. ; Torvik, P. J.: *A theoretical basis for the application of fractional calculus to viscoelasticity*. Journal of Rheology 27 (1983), Nr. 3, S. 201–210.

[5] Beyer, H. ; Kempfle, S.: *Definition of physically consistent damping laws with fractional derivatives*. ZAMM 75 (1995), Nr. 8, S. 623–635.

[6] Caputo, M. ; Mainardi, F.: *Linear models of dissipation in anelastic solids*. Rivista del Nuovo Cimento 1 (1971), Nr. 2, S. 161–198.

[7] Christensen, R. M.: *Theory of Viscoelasticity*. Academic Press, New York, 1971.

[8] Ferry, J. D. ; Landel, R. F. ; Williams, M. L.: *Extensions to the Rouse theory of viscoelastic properties to undiluted linear polymers*. Journal of Applied Physics 26 (1955), Nr. 4, S. 359–362.

[9] Gaul, L.: *The influence of damping on waves and vibrations*. Mechanical Systems and Signal Processing 13 (1999), Nr. 1, S. 1–30.

[10] Gaul, L. ; Bohlen, S. ; Kempfle, S.: *Transient and forced oscillations of systems with constant hysteretic damping*. Mechanics Research Communications 12 (1985), Nr. 4, S. 187–201.

[11] Gaul, L. ; Schanz, M.: *Dynamics of viscoelastic solids treated by boundary element approaches in time domain*. European Journal of Mechanics, A/Solids 13 (1994), Nr. 4, S. 43–59.

[12] Gaul, L. ; Schanz, M.: *A comparative study of three boundary element approaches to calculate the transient response of viscoelastic solids with unbounded domains*. Comput. Methods Appl. Mech. Engrg. 179 (1999), S. 111–123.

[13] Gemant, A.: *A method of analyzing experimental results obtained from elasto-viscous bodies*. Physics 7 (1936), S. 311–317.

[14] Gemant, A.: *On fractional differentials*. The Philosophical Magazine 25 (1938), S. 540–549.

[15] Graff, K. F.: *Wave Motion in Elastic Solids*. Dover Publications Inc., New York, 1975.

[16] Hilfer, R. (Hrsg.): *Applications of Fractional Calculus to Physics*. World Scientific, Singapore, 2000.

[17] Jones, D. I.: *Viscoelastic Vibration Damping*. John Wiley & Sons, New York, 2001.

[18] Koeller, R. C.: *Application of fractional calculus to the theory of viscoelasticity*. Journal of Applied Mechanics 51 (1984), S. 299–307.

[19] Lakes, R. S.: *Viscoelastic Solids*. CRC Press, Boca Raton, 1999.

[20] Lion, A.: *On the thermodynamics of fractional damping elements*. Continuum Mechanics and Thermodynamics 9 (1997), Nr. 2, S. 83–96.

[21] Oldham, K. B. ; Spanier, J.: *The Fractional Calculus*. Academic Press, New York and London, 1974.

[22] Padovan, J.: *Computational algorithms for FE formulations involving fractional operators*. Computational Mechanics 2 (1987), S. 271–287.

[23] Podlubny, I.: *Fractional Differential Equations*. Academic Press, San Diego and London, 1999.

[24] Rouse, P. E. J.: *The theory of linear viscoelastic properties of dilute solutions of coiling polymers*. The Journal of Chemical Physics 21 (1953), Nr. 7, S. 1272–1280.

[25] Schmidt, A.: *Finite-Elemente-Formulierungen viskoelastischer Werkstoffe mit fraktionalen Zeitableitungen*. Der Andere Verlag, Osnabrück, 2003. — Dissertation.

[26] Schmidt, A. ; Gaul, L.: *FE implementation of viscoelastic constitutive stress-strain relations involving fractional time derivatives*. In: *Constitutive Models for Rubber II*. A.A. Balkema Publishers, Tokyo, 2001, S. 79–89.

[27] Schmidt, A. ; Gaul, L.: *Finite element formulation of viscoelastic constitutive equations using fractional time derivatives*. Journal of Nonlinear Dynamics 29 (2002), S. 37–55.

[28] Schmidt, A. ; Gaul, L.: *On the numerical evaluation of fractional derivatives in multi-degree-of-freedom systems*. Signal Processing 86 (2006), Nr. 10, S. 2592–2601.

[29] Torvik, P. J. ; Bagley, R. L.: *On the appearance of the fractional derivative in the behavior of real materials*. Journal of Applied Mechanics 51 (1984), S. 294–298.

[30] VDI-Richtlinie 3830: *Werkstoff- und Bauteildämpfung. Blatt 2 — Dämpfung in festen Werkstoffen*. VDI-Verlag, Düsseldorf, 2004 (VDI Handbuch Schwingungstechnik, VDI-Handbuch Werkstofftechnik).

[31] VDI-Richtlinie 3830: *Werkstoff- und Bauteildämpfung. Blatt 5 — Versuchstechniken zur Ermittlung von Dämpfungskenngrößen*. VDI-Verlag, Düsseldorf, 2005 (VDI Handbuch Schwingungstechnik, VDI-Handbuch Werkstofftechnik).

[32] Wineman, A. S. ; Rajagopal, K. R.: *Mechanical Response of Polymers*. Cambridge University Press, Cambridge, 2000.

[33] Zimm, B. H.: *Dynamics of polymer molecules in dilute solution: viscoelasticity, flow birefringence and dielectric loss*. The Journal of Chemical Physics 24 (1956), Nr. 2, S. 269–278.